Instrumentation for the Measurement of Void-Fraction in Breaking Waves: Laboratory and Field Results

Eric Lamarre and W. Kendall Melville

Abstract—**We report on the development and use of an impedance probe to measure the volume fraction of air (void-fraction) in bubble plumes generated by breaking waves. The void-fraction gauge described here is found to be most useful in the initial period after breaking when large void-fractions prevail. We describe the instrumentation at length and report on its use in the laboratory and in the field. The instrument is found to be capable of rendering the space-time evolution of the void-fraction field from controlled laboratory breaking waves. Field results show measurements of void-fractions (up to 24%) which are several orders of magnitude greater than time averaged values previously reported [1], [2]. Preliminary measurements show that the fraction of breaking waves per wave, based on the detection of breaking by the void-fraction gauge, is dependent on significant wave height and wind speed. The dependence on wind speed is compared with data of previous investigators [3]. Underwater video photography from the field clearly shows the formation and evolution of distinct bubble plumes and the presence of large bubbles (at least 6-mm radius) generated by breaking.**

Keywords—**Breaking waves, void-fraction, bubble plumes.**

I. Introduction

WAVE breaking plays an important role in the physics and chemistry of the upper ocean. Breaking is an efficient mechanism for the dissipation of surface-wave energy [4]. Laboratory and field experiments have shown that the transfer rate of gases across an air–water interface increases significantly once breaking is initiated and bubbles are entrained [5], [6]. Ocean acousticians know that the wind-dependent ambient sound in the 1-kHz to 20-kHz range is due primarily to bubbles generated by breaking [7], and there is speculation that the wind dependence at lower frequencies (20 to 500 Hz) may be from the collective oscillations of bubbles [8]–[10]. Because of the presence of bubbles in the surface layer, the compressibility of the (air–water) mixture is increased, and therefore, the speed of sound is reduced. For example, a volumetric fraction of air of 1% in water reduces the sound speed by an order of magnitude (at ambient temperature and pressure) [11]. Farmer and Vagle [2] have reported on the effect of a reduced sound speed due to bubbles in the surface layers of the ocean. They have found it to be responsible for the presence of specific mode cutoffs in the sound spectrum from breaking waves. It is therefore evident that many physical and chemical processes in the upper ocean depend on the formation and transport of air bubbles from the air–sea interface into the oceanic surface layer (depth on the order of 10 m), and wave breaking is the primary mechanism for this "injection" of bubbles.

Several studies have been made in the laboratory and in the field on the bubble population from breaking waves. Most of the research has focussed on the time-averaged (over several wave periods) small-bubble population (less than 1.0-mm radius). Among the exceptional studies are the works by Medwin and his co-authors. In very gentle laboratory breaking waves, Medwin and Daniel [12] have studied the bubble population of individual breaking events over the full range of bubbles generated. Medwin and Breitz [13] have measured bubble population directly under breaking waves in the field but their study focused on bubbles with radii ranging from 0.03 mm to 0.27 mm. As the bubble population increases with more energetic breaking events, acoustic, photographic, and laser-based techniques reach a limit in their ability to distinguish the individual bubbles that make up the population. This is especially true when the bubble number density is large or consists of a wide range of bubble sizes.

The complex two-phase flow arising from breaking has made theoretical and experimental progress in this field difficult to realize. There is, therefore, a need for instrumentation capable of capturing useful information in the high void-fraction transient bubble plume generated by breaking. Air-entrainment measurements taken immediately after breaking make it possible to relate the characteristics of the bubble plume to the pre-breaking surface wave conditions [14].

In this paper we describe a device capable of measuring the volume fraction of air (void-fraction) in transient bubble plumes. The technique used to measure void-fraction is not novel but its application to unsteady free surface two-phase flows is new. We have previously reported on the results of laboratory experiments where the instrument was used [14]. Here we describe the technique and the instrument in detail and we also report on the first measurements of high void-fractions in the field. Low void-fractions in the ocean (10^{-6} to 10^{-8}) have been computed from time-averaged bubble populations in the past [1], [2], but no measurements of the high void-fractions (above 1%) in the transient bubble plume generated by breaking waves in the field have been previ-

Manuscript received October 23, 1991; revised December 13, 1991. This work was supported by the Office of Naval Research (Ocean Acoustics) and the National Science Foundation (Physical Oceanography).

The authors are with the R.M. Parsons Laboratory, Department of Civil Engineering, MIT, Cambridge, MA 02139.

IEEE Log Number 9106984.

0364-9059/92$03.00

ously reported. Such measurements are needed to test models of air entrainment, gas transfer, and low-frequency sound generation.

II. Instrumentation

A. Theory for the Determination of Void-Fraction by the Impedance Method

Maxwell [15, article 314] derived an expression for the effective conductivity σ_{eff} of a heterogeneous medium composed of noninteracting spheres of conductivity σ_1 dispersed in a medium of conductivity σ_2:

$$\sigma_{\text{eff}} = \frac{\sigma_1 + 2\sigma_2 + 2\alpha(\sigma_1 - \sigma_2)}{\sigma_1 + 2\sigma_2 - \alpha(\sigma_1 - \sigma_2)}\sigma_2 \tag{1}$$

where α is the volumetric fraction occupied by the spheres. For a mixture of air bubbles in water, the conductivity of the dispersed phase is much smaller than the conductivity of the medium, and Maxwell's expression reduces to

$$\sigma_{\text{eff}} = \frac{1-\alpha}{1+\alpha/2}\sigma_w \tag{2}$$

where σ_w is the conductivity of water. Maxwell's expression for σ_{eff} can be expanded to describe the effective permittivity, ϵ_{eff}, of the mixture

$$\epsilon_{\text{eff}} = \frac{1-\alpha}{1+\alpha/2}\epsilon_w \tag{3}$$

where ϵ_w is the permittivity of water. We have used in this last expression the fact that the permittivity of air is much smaller than the permittivity of water (by a factor of 80).

The impedance across two electrodes immersed in an air-water mixture can be modeled as a resistance, R, and a capacitance, C, in parallel:

$$R = \frac{K}{\sigma_{\text{eff}}}, \; C = \frac{\epsilon_{\text{eff}}}{K} \tag{4}$$

where K is the cell constant (with dimensions of length^{-1}) which is a function of the geometry and spacing of the electrodes. Because of fringing effects, the cell constant is often difficult to determine when working with finite size electrodes. Fringing occurs at the edges of the electrodes where the electric field is not uniform [16, pp. 173]. Using (2), (3), and (4), the total impedance for the parallel RC model can be written as

$$Z = \frac{K(1+\alpha/2)}{1-\alpha}\left(\frac{1}{\sigma_w} - \frac{j}{2\pi f \epsilon_w}\right) \tag{5}$$

where f is the electrode excitation frequency. The first term and second term in brackets are the real (resistive) and complex (capacitive) part of the impedance, respectively. Typical values for σ_w and ϵ_w for fresh water are 0.005 S/m and 7.1×10^{-10} F/m. Therefore, for $f \ll 1$ MHz, the fluid cell becomes resistive, and for $f \gg 1$ MHz it becomes capacitive. With an appropriate circuitry to measure resistance or capacitance, either regime could theoretically be used to measure void fraction but in practice it has been found difficult to eliminate capacitive pickup and electromagnetic radiation when operating in the capacitive mode [17].

When the fluid cell is excited by a direct current, the ions of the electrolyte accumulate on the solid electrodes and create an electromotive force acting in the opposite direction. This ionization of the water in the vicinity of the electrodes is known as polarization and it results in a diminution of current or an apparent increase in the resistance [15, article 264]. It is possible to significantly reduce the parasitic resistance due to polarization by exciting the fluid cell with an alternative current. The frequency of excitation is a function of the composition of the electrodes and of the electrolyte. Olsen [18] has found that polarization was eliminated with frequencies as low as 600 Hz for stainless steel electrodes immersed in fresh water. The polarization effect can be detected by monitoring the drift of the electronics' output when the electrodes are immersed in bubble-free water kept at constant temperature. If polarization is significant, it will show up as an apparent increase in the resistance of the fluid cell and will be detectable as drift at the electronics' output. A good example of this effect is an ohmmeter connected to two electrodes immersed in water. The meter will show immediate, steady increase in resistance until saturation of the instrument's output is reached.

B. Void-Fraction Instrumentation and Testing

In the experiments described here we used a Danish Hydraulic Institute Model 80-74a bridge designed for use with their resistive wire wave gauges. The excitation frequency was 3 kHz and the response of the circuitry was modified to be approximately flat out to 100 Hz (3-dB point).

Various electrode configurations were tested in order to find out the most suitable probe for void-fraction measurement in two-dimensional laboratory breaking waves. Our aim was to design a probe with minimum flow perturbation, temperature effect, surface effect, and bubble-size effect. Surface effect is due to the influence of the water surface on the electric field, and it restricts the ability of a probe to measure void-fraction close to the water surface. Bubble-size effect is due to the dependence of the instrument void-fraction output on bubble size. These effects will be discussed at length subsequently. Our final choice of electrode configuration is shown in Fig. 1(a). It consists of three parallel nichrome wires (0.127-mm diameter), 20 cm long and spaced 1.6 cm apart in a plane. Nichrome electrodes were selected because of our previous experience with them in resistive wire wave gauges. A frame made of 6-mm stainless steel tubing held the wires inside the wave channel. The two outer wires make up one electrode, while the inner one makes up the other. The wires are electrically isolated from the frame with Teflon fittings. Calibration of the void-fraction probe was performed in a cylindrical bubble tank (Fig. 1(b)) with adjustable bubble size and air-flow rate. The void-fraction in the bubble tank was measured by taking differential pressure measurements with an inverted air-on-water manometer. The manometer was an MKS model 310 pressure transducer equipped with an MKS type 170M-6B amplifier. Its resolu-

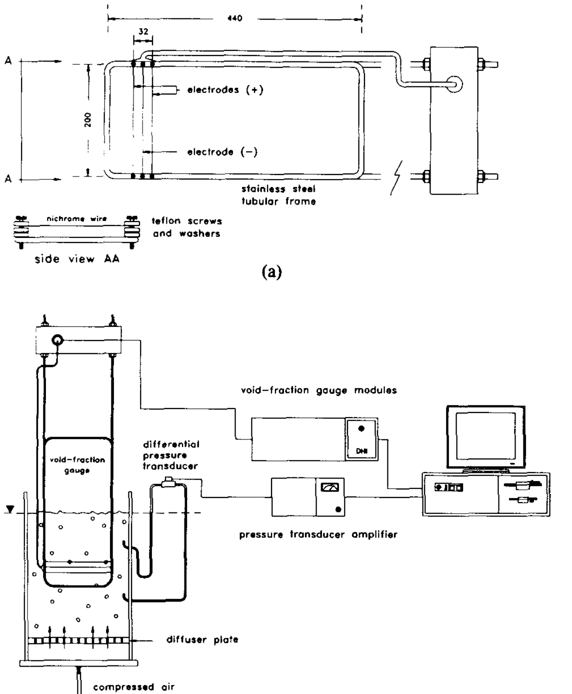

Fig. 1. (a) Void-fraction probe used in the laboratory experiments. (b) Calibration bubble tank and apparatus for the calibration of the void-fraction probe.

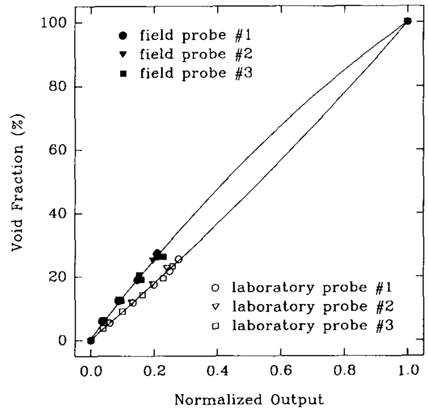

Fig. 2. Typical calibrations. The normalized output is given by $V^* = (V_w - V)/(V_w - V_a)$ where V is the voltage output from the instrument, V_w is the voltage in water only, and V_a is the voltage in air only. Direct calibrations up to 30% void-fraction were obtained along with calibration at 100% in air. Three laboratory probes (open symbols) and three field probes (filled symbols) were calibrated and used for the experiments. Data is fitted with second-order polynomials.

tion is 0.01% of the full range (1333 N/m^2) and its bandwidth was set to 0.04 Hz. At each specific air-flow rate, the manometer and the void-fraction gauge were sampled at 200 Hz, and a two-minute average was used to reduce the inherent fluctuations introduced by the two-phase flow. This long time-averaging of the calibration signal allowed us to assume a steady and uniform distribution of void-fraction between the two points where pressure measurements were taken, and therefore we obtain from fluid statics the following relationship for the void-fraction and the differential pressure:

$$\alpha(\%) = \left(1 - \frac{p_2 - p_1}{\rho_w g h}\right) 100 \qquad (6)$$

where $p_2 - p_1$ is the measured differential pressure between two points separated by a vertical distance h, ρ_w is the density of water, and g is gravity. The specific density of air has been neglected in (6) since it is very small compared to that of water. The probe has been calibrated for void-fractions up to 30%, and data at 100% were obtained by calibrating in air. The height of the reservoir (Fig. 1(b)) fixed the 30% upper-bound for tank calibration. Temperature changes of the water over the course of the entire calibration procedure were monitored and remained within +/− 0.5°C. Drift in the output of the manometer was recorded before and after each (two minutes) calibration point and was found to be negligible. Calibrations of the laboratory (fresh water) and field probe (to be discussed later) are shown in Fig. 2.

It should be pointed out that at low void-fraction (< 10%), the bubbles are essentially uniformly distributed throughout the entire calibration tank. At higher void-fraction, we have observed the formation of a 5–10 cm tall central bubble column located immediately above the diffuser plate with return flows on the sides of the tube. Above ~ 10 cm, we could not observe such organization anymore and the bubbles were essentially filling the full cross-section of the tube with no visible anisotropy. The taps for the differential pressure measurement (which yielded the void-fraction) were located at 14 and 34 cm above the diffuser plate, and the void-fraction probe was positioned at ~ 24 cm. Therefore, we do not believe that the calibration measurements could have been biased by an anisotropic organization of the bubbles inside the calibration tank.

The conductivity of bubble-free water is a strong function of temperature and salinity with temperature being more important in typical oceanic conditions. Generally speaking, this dependence varies on a very slow time scale (O(0.1°C/hr)) in water basins the size of a wave tank (or larger) compared to the larger and faster fluctuations in conductivity caused by air entrainment in breaking waves (order 1% void-fraction or more per second). Therefore, these slow changes due to temperature appear as dc offsets for the void-fraction measurements and can be easily subtracted from the signal. Nevertheless, breaking itself introduces small, local fluctuations in temperature, which occur on a fast time scale (comparable to void-fraction). These fluctuations have not been directly measured in bubble plumes immediately after breaking, but in the context of this work we can estimate them to be much less than 1°C from our knowledge of the total energy dissipated during breaking. Using a towed thermistor array, Thorpe and Hall [19] have measured the temperature anomalies due to bubble clouds at a depth of 0.9 m to 8.6 m and have found fluctuations on the order of 10 m°C. The dependence of the void-fraction measurement on temperature has been found by increasing the bubble-free water temperature from 14°C to 32°C and by recording the void-fraction gauge output. The equivalent void-fraction due to the temperature increase can be computed from the calibration, and it is shown in Fig. 3 where we find a bias of 0.4% void-fraction per degree Celsius. Since the void-fraction noise threshold of the laboratory probe described in this work is about 0.3%, we can therefore assume temperature fluctuations due to breaking to be negligible compared to void-fraction fluctuations.

A probe for free-surface void-fraction measurements must have a measuring volume small enough such that measurements close to the water surface can be made, but large enough to minimize the biasing effect of large bubbles. These two constraints will be referred to as surface effect and bubble-size effect. Surface effect occurs when the electric field induced by the electrodes is modified by the proximity of the water surface. A simple test was conducted in order to quantify this effect. The void-fraction probe was initially positioned at a depth of 10 cm in bubble-free water. It was then raised by 0.5-cm increments until the proximity of the water surface significantly changed the output. Fig. 4 shows the various electrode configurations tested and their dependence on the proximity of the water surface. The equivalent (bias) void-fraction output is plotted on the vertical axis. A comparison with a two-wire probe with the same electrode spacing shows the advantage of the three-wire probe in applications near the free surface. The measuring volume for the probe is approximately 20 cm long and of elliptic cross-section. The depths at which the surface effect become significant define the transverse dimensions of the measuring volume. The open circle symbols give the dimensions of the semi-major axis (~ 2.5 cm based on a 0.3% threshold) and the open square symbols give the dimensions of the semi-minor axis (~ 1.8 cm). These dimensions for the measuring volume are of the same order as the value calculated by Hill and Woods [20] for the two-point electrode configuration with similar electrode spacing.

An ideal probe would give the same void-fraction independently of the bubble size distribution. In reality, the effect of bubble size becomes negligible only if the diameter of the bubbles (d) is about an order of magnitude smaller than the spacing between the electrodes (D) [18]. Bubbles of various diameters can be generated in the bubble tank by changing the hole size in the diffuser plate, and their diameter can be measured from video images at low void-fraction. Fig. 5 shows calibration of the probe for two different bubble sizes. If we assume that calibrations with 1.5-mm radius bubbles ($d/D = 0.19$) have negligible bubble effect, we can therefore estimate the bias error for 5-mm radius bubbles ($d/D = 0.63$) to be about 10% of the void-fraction reading. In our study of bubble-size effect, we have tried several other techniques to generate bubbles with radius smaller than 1.5 mm. A solution of 10% by volume of isopropyl alcohol was used to reduce the surface tension but the bubble size reduction was not significant. A fine wire mesh placed on top of the diffuser plate did not help in splitting up the bubbles. Much smaller bubbles could be generated by hydrolysis but their number density was too low to build up to a detectable

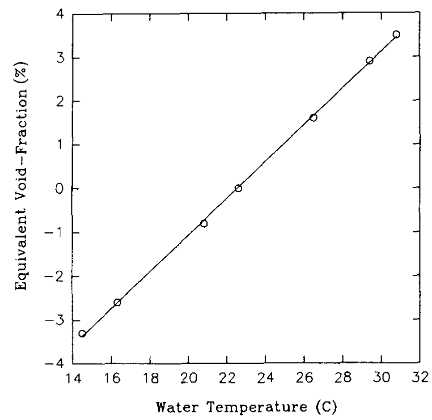

Fig. 3. Dependence of void-fraction measurement on water temperature. The equivalent void-fraction output from the instrument is plotted as a function of the water temperature. The zero point has been arbitrarily set at 22.6°C.

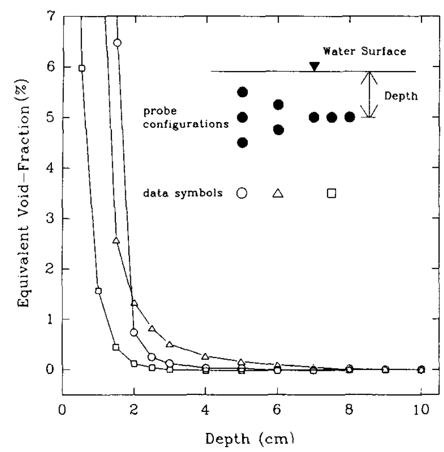

Fig. 4. Surface effect. When the free surface is too close to the measuring volume, the void-fraction measured by the instrument is biased by the free surface. The diagram in the upper right-hand corner shows how the depth was measured for the various electrode configurations.

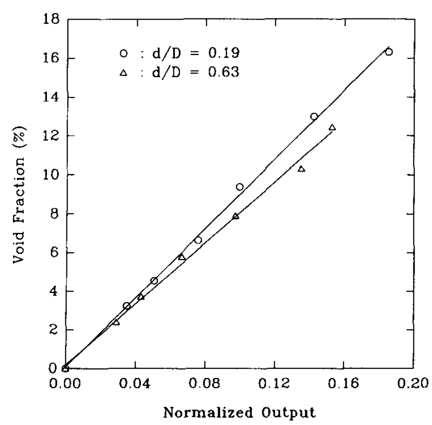

Fig. 5. Calibration of the void-fraction probe for two different bubble sizes. The ratio of the bubble diameter to the electrode spacing is given by the parameter d/D.

void-fraction level. We have been unable to test a porous glass membrane (with nitrogen bubbles) because of the difficulty in obtaining a membrane 24 cm in diameter (size of the calibration tank) and capable of supporting the pressure necessary to drive the gas bubbles through it.

In our attempt to find a way to eliminate bubble-size effect, we have experimented with a void-fraction gauge made out of two circular stainless steel electrodes 2.5 cm in diameter spaced by 10 cm. These dimensions were chosen to approximately match the dimensions of the measuring volume of the void-fraction "wire" gauge. We have found the "plate" gauge to be insensitive to bubble-size effect as expected for $d/D = 0.1$ (bubble diameter $d = 1$ cm and electrode spacing $D = 10$ cm). Unfortunately, surface effects due primarily to fringing were found to be significant for depths comparable to the electrode spacing. Furthermore, flow perturbation was increased by the necessity for a bulkier supporting frame for the deployment of the electrodes. In the end, the "wire" gauge was chosen to minimize the surface effect at the expense of a possible 10% (of the void-fraction reading) bias error due to bubble-size effect.

C. Wave Generation

The experiments were conducted in a glassed-wall wave channel 25 m long and 0.7 m wide filled to a depth of 0.6 m. The breaking waves were produced with a piston-type wavemaker by generating a packet of waves with progressively decreasing frequencies. The dispersive properties of water waves focus the packet at a predetermined position down the channel. The wave packets studied in the laboratory experiment were composed of 32 sinusoidal components of equal slope $a_i k_i$ where a_i and k_i are the amplitude and wavenumber of each component. The wave packet generation technique is discussed at length in Rapp and Melville [21]. Excellent repeatability of the wave profile is shown in Fig. 6(a) where wave gauge time-series (5 cm upstream of breaking) of 60 repeats of the same breaking wave packet are shown. The repeatability of the void-fraction measurements were found to be relatively good as shown in Fig. 6(b) where the mean of 20 ensemble averages (each ensemble is the average of three repeats) of void-fraction time-series at the center of the bubble plume is plotted along with $+/-$ one standard deviation of the 20 ensembles. The probe was positioned inside the channel with the long axis of its measuring volume spanning the width of the tank. Video imaging from the side of the wave channel, and under water, showed that the large-scale features of the bubble plume were repeatable and essentially two-dimensional.

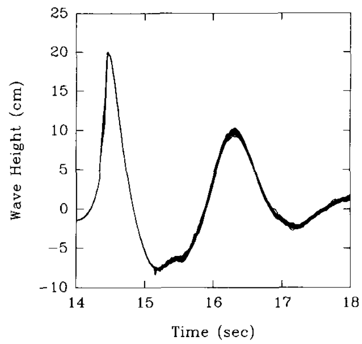

(a)

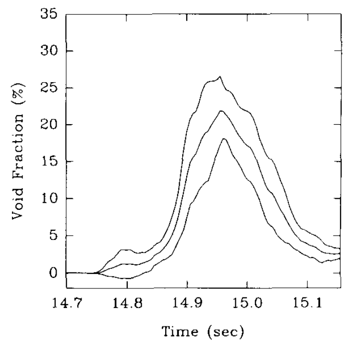

(b)

Fig. 6. (a) Sixty wave-gauge time-series 5 cm upstream of breaking for the same experiment. The larger differences at later times are due to short waves generated by the breaking wave moving upstream towards the wave gauge. (b) This plot shows the typical repeatability of the void-fraction measurement. The mean of 20 ensemble averages of three runs is plotted along with $+/-$ one standard deviation of the 20 ensembles.

D. Additional Instrumentation

Resistive wire wave gauges were used to give the wave profile at several locations along the wave channel. The probes were built at MIT and consist of two parallel Nichrome wires (0.127 mm diameter) 45 cm long spaced by 4 mm. The electronic circuits are commercial units from the Danish Hydraulic Institute (model 80-74G). An NEC TI-23A 1/2-in format CCD video camera with 1/1000-s shutter speed was used to produce video images of the position of the probes with respect to the bubble plume and the water surface. The camera was equipped with Fujinon lens model CF12.5A and CF25B. The video images were run through a Datum 9300A time code generator before being recorded on a Panasonic AG-6300 VHS video recorder. A Hasselblad 500EL/M camera was used for still photography. The lighting technique was similar to the one used by Rapp [22]. Acquisition of wave gauge and void-fraction gauge data was synchronized with the wave maker, the time code generator, and the camera (when used), to establish a common time basis for all experiments. Wave gauges and void-fraction gauges were mounted on a carriage which was moved along the wave channel by a synchronous stepping motor manufactured by Superior Electric (model M061-FD02). The motor was computer controlled by a Superior Electric model STM200 translator module and a Metrabyte PIO-24 digital I/O card, and therefore, the numerous repeats of the experiment could be automated.

III. Laboratory Experiments

A. Mapping of the Void-Fraction Field and Comparisons with Photographs

The void-fraction field of a bubble plume generated by an energetic breaking wave was measured and compared with still photographs of the plume. The wave packet center frequency was 0.78 Hz with a bandwidth of 0.57 Hz and a slope $ak = 0.54$ (see [21] for more details on the generation of the wave packet). A single breaker was generated downstream at 9.6 m from the wavemaker. Three void-fraction gauges and three wave gauges were used along with the video camera for each run. The breaking region was surveyed by the void-fraction probes with a grid spacing of 10-cm increments along the channel and 5-cm increments in depth. Three repeats at the same position in the channel were ensemble averaged to reduce the variance of the void-fraction measurements. Approximately 170 ensemble averages were necessary to map out the entire bubble plume along with the position of the free surface. The data was then edited to eliminate the transitions where the void-fraction probe crossed the free-surface. Video imaging of the void-fraction probes from the side of the channel helped in this task. Color contour maps of the void-fraction field were then reconstructed from the individual ensemble averages since all repeats were on the same time basis. Raw data was time-averaged over a 0.05-s window and gridded on a finer 2-cm by 1-cm mesh using a Laplacian and spline scheme [23]. Fig. 7 shows color contour maps of the void-fraction field and still photographs of the wave profiles and bubble plumes at various times. There is good agreement between the bubble plume cross-sectional area on the color contours and the photographs. Void-fractions below 0.3% were below the detection threshold of the instrument and could not be resolved. We have observed that bubbles located in the close vicinity (approximately 5 cm or less) of the vertical walls tend to get trapped, with their velocities significantly reduced in this boundary layer. This effect is more apparent when the bubbles rise back to the surface since it will cause the bubbles close to the wall to reside in the water longer. Photographs from the side of the channel (last frame of Fig. 7) show an apparently larger bubble plume (especially at later times) than what is actually present and measured by the void-fraction probe at the center of the channel.

B. Experiments on Three Wave Packet Amplitudes

The success of our initial tests in accurately reproducing the void-fraction field led us to take on a more comprehensive set of experiments where the dependence of air entrainment parameters on the dynamical wave parameters were studied. The results obtained by taking various moments of the void-fraction field are discussed in Lamarre and Melville [14]. The main conclusions are that the important parameters describing the bubble plume generated by breaking, namely the volume of air, the cross-sectional area, the potential energy, and the mean void-fraction of the plume, all evolve according to simple functions of time. Mean bubble plume void-fractions above 1% are sustained for a full wave period after breaking is initiated. Of particular interest is the fact that the energy required to entrain the bubbles against buoyancy represents a significant fraction (30–50%) of the total energy dissipated by breaking. These laboratory experiments showed the capabilities of the void-fraction measurement technique for measuring air entrainment in bubble plumes generated by breaking waves.

IV. Field Test

A. The Probe

A field version of the void-fraction gauge was tested during the Surface Wave Dynamics Experiment (SWADE). The conductivity of sea water is approximately three orders of magnitude larger then the conductivity of fresh water. It was clear that modifications to the electronics or the probe would be needed to optimize the void-fraction instrumentation for sea conditions. Two 6-mm diameter stainless steel electrodes 30 cm long were embedded in 10-mm nonconducting glass reinforced epoxy tubes. A 4-cm long by 4-mm wide incision was made in each of the tubes to expose the electrodes to the sea water. This masking was found to significantly increase the cell constant and permitted the operation in sea water with unmodified circuitry. The electrodes were mounted 10 cm apart on a small glass reinforced epoxy waterproof enclosure. The field probe was post-calibrated in the calibration tank (Fig. 1(b)) with sea water from the test site. Calibrations are shown in Fig. 2. The noise threshold of the field probe was found to be no more than 0.3% void-fraction, with some electronic modules showing better characteristics than others. Surface effects were found to be negligible when the probe's top electrode was located at a 6-cm depth. Bubble-size effects were not investigated for the field probe since the ratio of the largest bubbles encountered in the video to the electrode spacing (i.e., d/D) was about 0.1 (cf., Section II-B.).

B. The Buoy and Its Instrumentation

A buoy was built to carry three void-fraction probes, one B&K model 8103 omnidirectional hydrophone, and an NEC TI-23A video camera (with a Fujinon model HF4.8B-SND4-1 auto-iris lens) mounted in an underwater housing fabricated by Underwater Video Vault (Spring, Texas). Fig. 8(a) shows a line drawing of the buoy and its apparatus, and Fig. 8(b) shows the buoy on the deck of the Research Vessel Cape Henlopen from which it was deployed approximately 100 km off the coast of Delaware during the last week of February 1991. The void-fraction probes were installed at a depth of 20, 50, and 80 cm from the water surface (depth is measured from the center of the electrodes). The hydrophone was deployed at 1 m below the surface and the video camera at 20 cm. All signals were carried back to the ship by a set of five 100-m cables which were supported along their length by small floats. The buoy was deployed upwind of the ship, and the ship was maneuvered to keep the tether slack.

C. Results

We have analyzed 465 min of data from a total of 560 min acquired during the three days of the field test. The wind and significant wave height ranged from 4.5 m/s to 14.9 m/s and 1.7 m to 2.8 m, respectively. The wind was measured at 4 m and estimated at 10 m using a logarithmic profile with drag coefficient for neutral conditions [24]. The wind and wave conditions along with the date and duration of the three deployments are reported in Table I. Each deployment is divided into hourly intervals to match the hourly data from

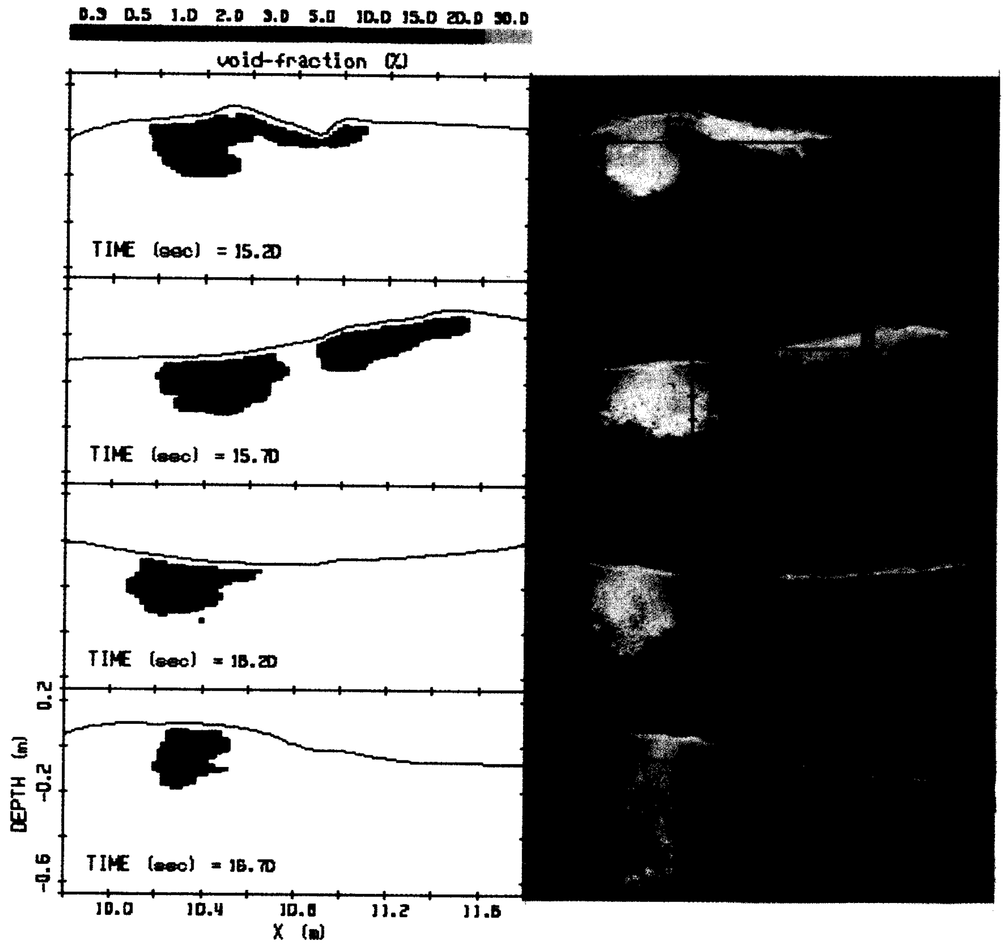

Fig. 7. Color contour maps of laboratory measurements of the void-fraction field at four different times along with matching photographs of the breaking wave and the entrained bubble plume. The center line of the photographs is at 10.5 m from the paddle. The still water level is the horizontal line. Time is from the start of the paddle motion.

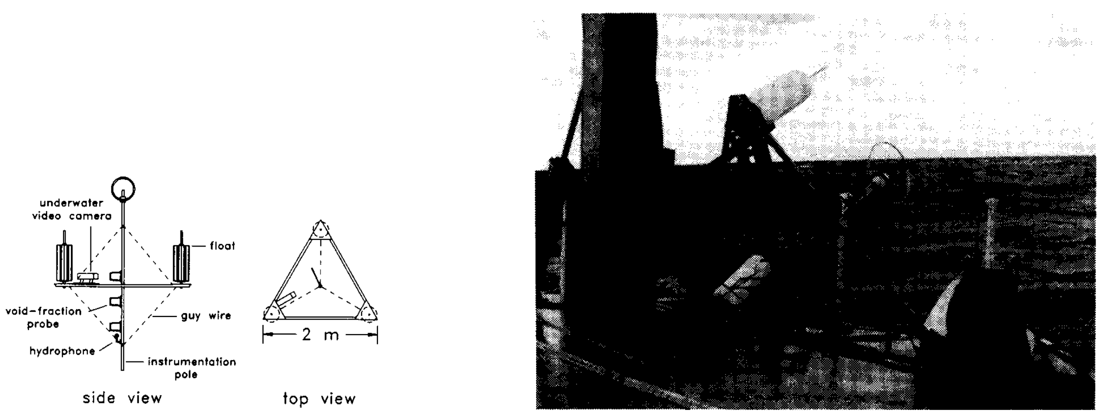

(a)

(b)

Fig. 8. (a) Line drawing of the buoy and associated instruments. (b) Photograph of the buoy and the mounted equipment on the deck of the R/V Cape Henlopen.

TABLE I
THREE DEPLOYMENTS DURING THE SWADE FIELD TEST

Deployment #	Date	Time (EST)	Duration (min)	U_{10} (m/s)	SWWH (m)	T_{dom} (s)	V.F. #	α (%)
1	02-25-91	9:00	55	14.1	2.7	8.3	20	5.0
		10:00	55	13.1	2.7	8.3	22	5.5
		11:00	45	13.4	2.8	6.2	33	7.6
2	02-26-91	9:00	60	4.5	1.7	8.3	10	2.3
		10:00	55	8.0	1.8	7.1	11	2.4
		11:00	40	6.6	1.7	8.3	5	1.7
3	02-27-91	12:00	35	14.9	2.4	6.7	9	2.9
		13:00	60	14.1	2.8	6.2	34	5.9
		14:00	60	13.1	2.7	6.7	30	5.6

Wind speed, significant wave height (SWH) and dominant wave period (T_{dom}) are from nearby SWADE buoys located no further than 8 km away. Wind speed was measured at 4 m and estimated at 10 m (U_{10}) using a logarithmic wind profile with a drag coefficient for neutral conditions [24]. Wind speed was averaged over 8 min, and significant wave height and dominant wave period are 20-min averages. The fraction of breaking waves per wave (α) is obtained from the number of void-fraction (VF) events above 1% divided by the duration multiplied by the dominant wave period. Eastern standard time is with respect to the center of the hourly record.

SWADE buoys located no further than 8 km away. Wave breaking conditions were sufficiently strong to provide void-fraction measurements and video images of occasional large-scale bubble plumes. The underwater video photography provided impressive visualization of the formation and evolution of the bubble plume. The video camera looked horizontally at the probe located at a depth of 20 cm. The housing was equipped with an 8-cm diameter Plexiglass dome port as the water interface lens. The dome port creates a virtual image of the real object being observed. This image is 2–20 cm in front of the dome, depending on the distance of the real object (from the dome to infinity). The camera was mounted with a lens having a 4.8-mm focal length and a measured 18-cm depth of field. Therefore, by focussing the camera at 11 cm everything in front of the dome port appears in focus. Fig. 9 displays photographs taken from the underwater video tape. They were generated by taking photographs (Kodak Plus-X pan 125 film at a 1/15 s shutter speed and 5.6 aperture) of a 38-cm Panasonic WV-5470 video monitor with the recorder set on still mode. The photographs clearly show the birth and evolution of a bubble cloud. The section of the frame's horizontal member shown at the bottom of the photographs measures approximately 1.2 m and is located 1.1 m in front of the camera at a depth of 0.4 m. The series of photographs in Fig. 9 correspond to a time-series from the upper void-fraction probe shown on Fig. 10(d) (the arrow on Fig. 10(d) corresponds to frame 8 of Fig. 9).

The video also permitted the observation of large bubbles. Their minimum dimensions were inferred from the known diameter of the dome port (8 cm). Fig. 9 (frames 5, 6, and 7) shows large bubbles from the breaking event with the largest for this event being 5 mm in radius (frame 7). In almost every situation where bubbles reached the front of the dome port, it was possible to identify bubbles with radii in the millimeter range. Unfortunately, the bubble population in that range has not yet been quantified either in the field or in the laboratory, and we believe this has impeded our understanding of a number of physical processes, including sound generation and gas transfer.

The objective of the field test was to demonstrate the feasibility of the impedance technique for the measurement of void-fraction in the field and to show that large void-fractions can be encountered in the bubble plumes generated by breaking. Our data set is sparse and limited to moderate breaking conditions. A 1-min time-series extracted from a 5-min record is shown in Fig. 10(a) for the gauge at 20 cm. The record is from the third deployment at 14:00 hours (see Table I). Void-fraction events above a threshold of 0.5% are found to be intermittent, with no events occurring in the remaining four minutes of the record. Shorter time-series (11 s) from the gauge at 20 cm (Fig. 10(b) and (c)) show details of the void-fraction signal for multiple events. The signal characteristically shows large variations in amplitude and duration. Large-scale void-fractions up to 24% are shown in the short time-series of Fig. 10(d). The arrow on Fig. 10(d) corresponds to frame 8 of Fig. 9. Very few events of high void-fraction have been detected in the time-series at 50 cm (10 for all three deployments) with the highest one being 5% (Fig. 10(e)). None were detected at 80 cm. We have been unable to detect simultaneous measurement of void-fraction events on separate gauges. This may be because of the limited data available at 50 cm and the relatively large separation between the top and middle gauge (30 cm). The high void-fractions of Fig. 10(d) are consistent with the laboratory results described earlier and are several orders of magnitude higher than time-averaged values reported from the field [1], [2]. We have processed the time-series to give the signal duration and the maximum void-fraction for every event above a 0.5% threshold. An event is defined by a signal above the threshold and individual events are set apart when the signal returns below the threshold. The results are shown in the scatter plots of Fig. 11. Deployments 1 and 3, which had similar wind speed and significant wave height, also show similar scatter plots (Fig. 11(a) and (c)). Significantly fewer occurrences were observed for the second deployment (Fig. 11(b)) where both the wind speed and the significant wave height were noticeably lower.

The field version of the void-fraction gauge can also be used to extract quantitative information on the statistics of breaking waves. Toba [25] and Holthuijsen and Herbers [3] have quantified the fraction of breaking waves per wave (hereafter, fraction of breaking waves) by using the presence of a whitecap at a fixed point on the surface. Similar measurements using the time derivative of a wave gauge signal have been made by Thorpe and Humphries [26] and Longuet-Higgins and Smith [27]. Holthuijsen and Herbers [3] have reported on the significant differences in the above studies when correlating the fraction of breaking waves with wind speed. They have attributed the differences to the detection technique and its associated definition of breaking.

When used as a detector of breaking waves, the void-fraction should ideally be located very close to the surface. The minimum depth at which the probe can be deployed is restricted by surface effect and we can expect that there will always be some gently breaking waves that will not penetrate the minimum depth. The effect of the probe's depth will be to underestimate the fraction of breaking waves. The number of

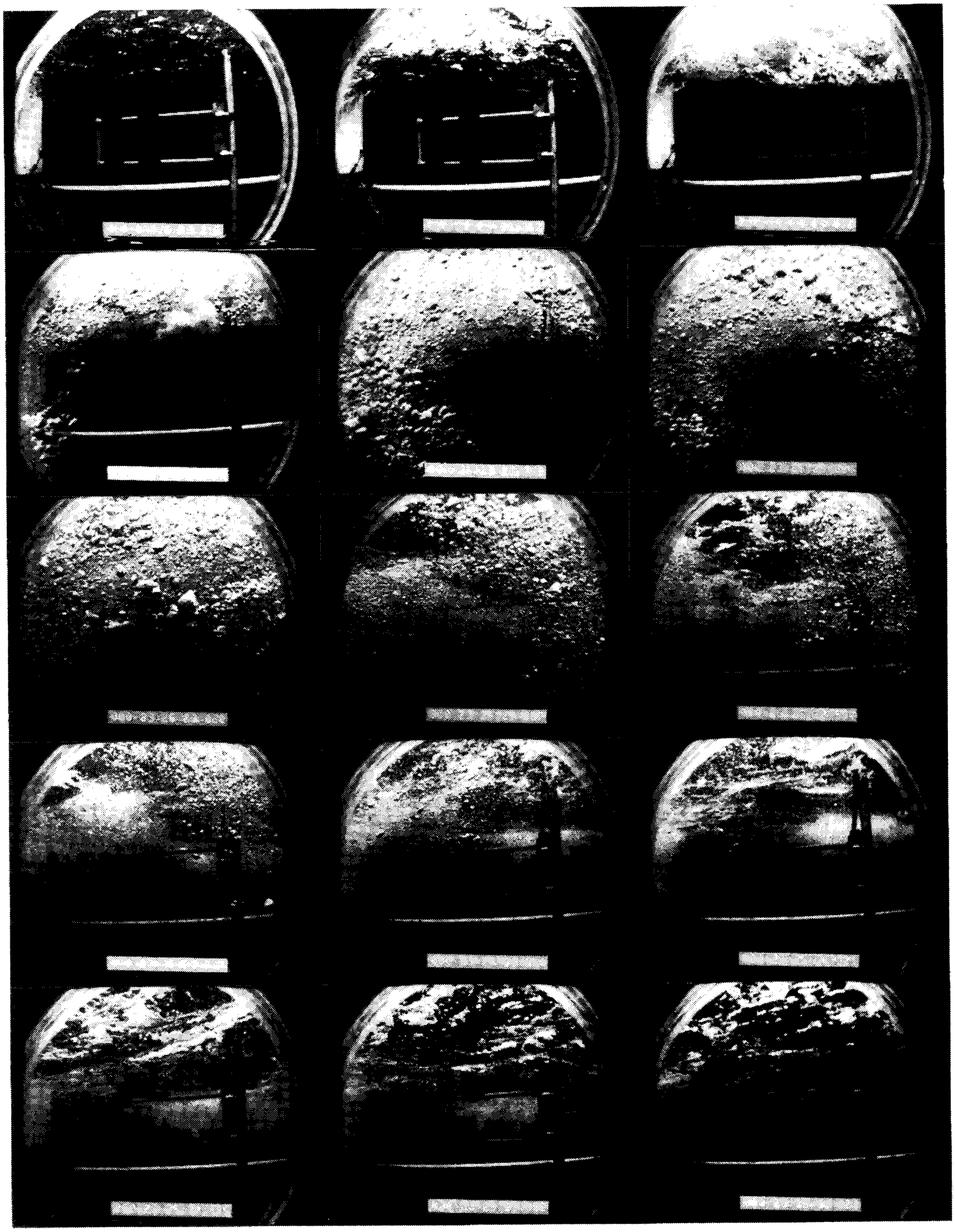

Fig. 9. Photographs of the bubble plume taken from the video recording. The photographs evolve in time from left to right and from top to bottom. Frames 1–7 are 0.133 s apart, frames 7–12 are 0.267 s apart, and frames 12–15 are 0.533 s apart. Frame 8 corresponds to the arrow on Fig. 10(d). The largest bubble (5-mm radius) in this sequence is seen in frame 7.

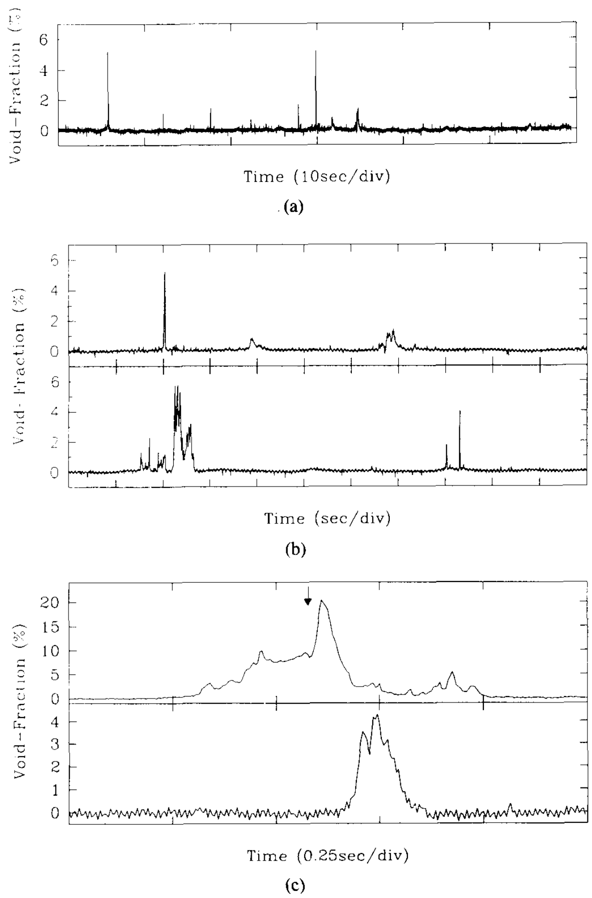

Fig. 10. (a) A 1-min record of the void-fraction signal. (b) Enlarged middle section of the time-series in (a). (c) Time-series with multiple events showing a wide range of signal amplitude and duration. (d) Short time-series showing large void-fraction signal. The arrow corresponds to frame 8 of Fig. 9. (e) Time-series for the gauge at 50 cm. All other time-series are for the gauge at 20 cm. Data sampled at 200 Hz.

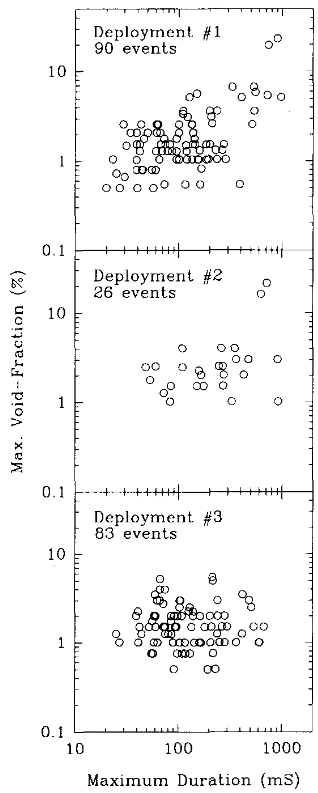

Fig. 11. Scatter plots of event time duration versus maximum void-fraction for (a) deployment #1, (b) deployment #2, and (c) deployment #3. Each deployment has a duration of 155 min. The void-fraction is the maximum to occur for each event and the time duration is the total time of the event above a threshold of 0.5% void-fraction. Note that one breaking wave may lead to multiple events (cf., Fig. 10(c)) so the time-duration should not be interpreted as the duration of a breaking wave.

void-fraction events above a 1% threshold are reported in Table I. In some time-series (Fig. 10(c)), we have observed multiple events that occur on a time scale much shorter than a typical wave period. These events are probably from the same breaking wave, and therefore, this simple detection scheme may tend to overestimate the fraction of breaking waves. The difficulty of discriminating between breaking and nonbreaking events is a familiar problem in the study of breaking wave statistics [3] both from an instrumentation and from a definition point of view. Our preliminary aim in this paper is to present the impedance technique as a way of measuring void-fractions in bubble plumes generated by breaking waves. More sophisticated detection schemes and more data are required for a detailed study of breaking wave statistics.

With this simple detection scheme the fraction of breaking waves is given by the number of void-fraction events per second multiplied by the dominant wave period (Table I). Fig. 12(a) shows the fraction of breaking waves as a function of wind speed. Our data shows scatter comparable to previous studies and is consistent with results based on the time derivative of a wave gauge signal [26], [27]. It may be that our results are more compatible with the above two studies because the time derivative technique tends to detect events associated with rapid changes in the surface elevation, which may lead to a greater penetration of the bubble plume. Fig. 12(b) shows the fraction of breaking waves as a function of significant wave height. There is clearly an increase with significant wave height but the relatively small data set limits the significance of the correlation. Attempts to correlate the fraction of breaking waves with wind speed and significant wave height for higher thresholds of the void-fraction signal (3% and 5%) were less successful because of the limited number of events at these higher thresholds. We found no significant changes in the results of Fig. 12(a) and (b) for lower thresholds down to 0.5% void-fraction.

V. Conclusions

We have reported on an effective instrument for the measurement of void-fraction in breaking waves and related free surface two-phase flows. Surface effects and bubble-size ef-

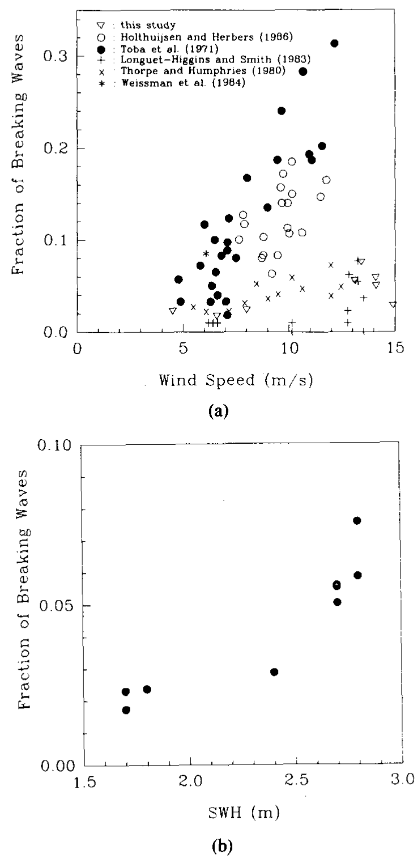

Fig. 12. Fraction of breaking waves per wave as a function of (a) wind speed (adapted from Holthuijsen and Herbers [3]), and (b) significant wave height (SWH).

fects have been shown to be important characteristics of the probe while temperature effects are found to be negligible for large void-fractions (above 0.3%). We have shown that the instrument can accurately map out the void-fraction field in laboratory breaking waves, especially in the initial wave period following onset of breaking, and that valuable information can be extracted from the void-fraction field [14]. A field version of the instrument has revealed high void-fraction measurements consistent with the laboratory data and several orders of magnitude larger than the time-averaged values previously reported. Void-fraction events above a threshold of 0.5% were found to be sporadic at a depth of 20 cm, and no occurrences have been detected at 80 cm for the three deployments reported here. The number of events at 20-cm depth increases with increasing sea state but their duration and their maximum void-fraction did not significantly change with sea state. The fraction of breaking waves detected by the void-fraction gauge as a function of wind speed is found to be consistent with lower bound data of previous studies. Future work at sea should include measurements of void-fractions in the 10^{-5} to 10^{-3} range, which corresponds to a regime of sharp reduction in the sound speed (from 1356 m/s to 311 m/s). Video photography has shown frequent occurrences of large bubbles (at least 6-mm radius) in the field. Their population remains to be measured if we are to understand their contribution to low-frequency ambient sound spectrum and air-sea gas transfer.

Acknowledgment

The authors thank Professor H. Kytömaa of MIT for helpful advice in the initial stage of this work and Paul Greenberg for his assistance in the analysis of the field data. We also thank Dave Oberholtzer of the Observational Science Branch of NASA for providing us with wind and wave data from nearby SWADE buoys.

References

[1] A. L. Walsh and P. J. Mulhearn, "Photographic measurements of bubble populations from breaking wind waves at sea," *J. Geophys. Res.*, vol. 92, pp. 14553-14565, 1987.

[2] D. M. Farmer and S. Vagle, "Waveguide propagation of ambient sound in the ocean surface bubble layer," *J. Acoust. Soc. Am.*, vol. 86, pp. 1897-1908, 1989.

[3] L. H. Holthuijsen and T. H. C. Herbers, "Statistics of breaking waves observed as whitecaps in the open ocean," *J. Phys. Oceanog.*, vol. 16, pp. 290-297, 1986.

[4] W. K. Melville and R. F. Rapp, "Momentum flux in breaking waves," *Nature*, vol. 317, pp. 514-516, 1985.

[5] L. Merlivat and L. Memery, "Gas exchange across an air-water

interface: experimental results and modeling of bubble contribution to transfer," *J. Geophys. Res.*, vol. 88, pp. 707-724, 1983.
[6] A. J. Watson, R. C. Upstill-Goddard, and P. S. Liss, "Air-sea exchange in rough and stormy seas measured by the dual-tracer technique," *Nature*, vol. 349, pp. 145-147, 1991.
[7] H. Medwin and M. M. Beaky, "Bubble sources of the Knudsen sea noise spectra," *J. Acoust. Soc. Am.*, vol. 86, pp. 1124-1130, 1989.
[8] A. Prosperetti, "Bubbly dynamics in oceanic ambient noise," in *Sea Surface Sound*, B. R. Kerman, Ed. Dordrecht: Kluwer, pp. 151-171, 1988.
[9] W. M. Carey and D. Browning, "Low frequency ocean ambient noise: Measurements and theory" in *Sea Surface Sound*, B. R. Kerman, Ed. Dordrecht: Kluwer, pp. 361-376, 1988.
[10] S. W. Yoon, L. A. Crum, A. Prosperetti, and N. Q. Lu, "An investigation of the collective oscillations of a bubble cloud," *J. Acoust. Soc. Am.*, vol. 89, pp. 700-706, 1991.
[11] A. B. Wood, *A Textbook of Sound*. London: G. Bell and Sons, 1941.
[12] H. Medwin and A. C. Daniel Jr., "Acoustical measurements of bubble production by spilling breakers," *J. Acoust. Soc. Am.*, vol. 88, pp. 408-412, 1990.
[13] H. Medwin and N. D. Breitz, "Ambient and transient bubble spectral densities in quiescent seas and under spilling breakers," *J. Geophys. Res.*, vol. 94, pp. 12 751-12 759, 1989.
[14] E. Lamarre and W. K. Melville, "Air entrainment and dissipation in breaking waves," *Nature*, vol. 351, pp. 469-472, 1991.
[15] J. C. Maxwell, *A Treatise on Electricity and Magnetism*. Oxford: Clarendon, 1892, vol. 1.
[16] M. Zahn, *Electromagnetic Field Theory*. Malabar, FL: Krieger, 1979.
[17] J. E. Rubesch, *The Design of a Hybrid Resistance-Capacitance 50 MHz Impedance Void-Fraction Meter*. Cambridge, MA: Massachusetts Institute of Technology, 1990.
[18] H. O. Olsen, *Theoretical and Experimental Investigation of Impedance Void Meters*, Kjeller Research Establishment, University of Oslo, Norway, 1967.
[19] S. A. Thorpe and A. J. Hall, "Bubble clouds and temperature anomalies in the upper oceans," *Nature*, vol. 328, pp. 48-51, 1987.
[20] K. D. Hill and D. J. Woods, "The dynamic response of the two-electrode conductivity cell," *IEEE J. Ocean. Eng.*, vol. 13, pp. 118-123, 1988.
[21] R. J. Rapp and W. K. Melville, "Laboratory measurements of deep water breaking waves," *Phil. Trans. R. Soc. Lond.*, vol. A331, pp. 735-800, 1990.
[22] R. J. Rapp, *Laboratory Measurements of Deep Water Breaking Waves*. Cambridge, MA: Massachusetts Institute of Technology, 1986.
[23] T. L. Young and M. L. Van Woert, *Plot88 Software Library Reference Manual*, Ramona, CA, Plotworks, 1989.
[24] W. G. Large and S. Pond, "Open ocean momentum flux measurements in moderate to strong winds," *J. Phys. Oceanog.*, vol. 11, pp. 324-336, 1981.
[25] Y. H. Toba, K. Kunishi, S. Nishi, S. Kawai, Y. Shimada, and N. Shibata, "Study on air-sea boundary processes at the Shirahama Oceanographic Tower Station," Disaster Prevention Institute, Kyoto Univ. Annals, vol. 148, pp. 519-531, 1971.
[26] S. A. Thorpe and P. N. Humphries, "Bubbles and breaking waves," *Nature*, vol. 283, pp. 463-465, 1980.
[27] M. S. Longuet-Higgins and N. D. Smith, "Measurement of breaking waves by a surface jump meter," *J. Geophys. Res.*, vol. 88, pp. 9823-9831, 1983.

Eric Lamarre received the B.Eng. degree in civil engineering and applied mechanics in 1988 from McGill University, Montreal.

He is currently working towards a Ph.D. in the MIT/WHOI joint program in civil and oceanographic engineering. His research interests include air entrainment in breaking waves, underwater sound propagation, long-wave-short-wave interaction, and radar altimetry.

W. Kendall Melville received the B.Sc. in mathematics in 1966, and the B.E. and M.Eng.Sc. degrees in aeronautical engineering in 1968 and 1970, respectively, from the University of Sydney, and the Ph.D. degree in aeronautics from the University of Southhampton in 1974.

Following a postdoctoral fellowship at the University of New South Wales, he moved to the Institute of Geophysics and Planetary Physics, U.C. San Diego, in 1977. Since 1980 he has been on the faculty of the R.M. Parsons Laboratory, Department of Civil Engineering, Massachusetts Institute of Technology. His research interests include fluid mechanics, air-sea interaction, surface wave stability and breaking, acoustical oceanography, microwave remote sensing, and nonlinear internal waves.